ORGANOMETALLICS

Article

pubs.acs.org/Organometallics

Ligand Tuning in Pyridine-Alkoxide Ligated Cp*Ir^{III} Oxidation Catalysts

Emma V. Sackville,[†] Gabriele Kociok-Köhn,[‡] and Ulrich Hintermair*[,†]

[†]Centre for Sustainable Chemical Technologies, University of Bath, Claverton Down, Bath BA2 7AY, United Kingdom

[‡]Chemical Characterisation and Analysis Facility, University of Bath, Claverton Down, Bath BA2 7AY, United Kingdom

Supporting Information

ABSTRACT: Six novel derivatives of pyridine-alkoxide ligated Cp*Ir^{III} complexes, potent precursors for homogeneous water and C−H oxidation catalysts, have been synthesized, characterized, and analyzed spectroscopically and kinetically for ligand effects. Variation of alkoxide and pyridine substituents was found to affect their solution speciation, activation behavior, and oxidation kinetics. Application of these precursors to catalytic C−H oxidation of ethyl benzenesulfonate with aqueous sodium periodate showed that the ligand substitution pattern, solution pH, and solvent all have pronounced influences on initial rates and final conversion values. Correlation with O_2 evolution profiles during C−H oxidation catalysis showed these competing reactions to occur sequentially, and demonstrates how it is possible to tune the activity and selectivity of the active species through the N^O ligand structure.

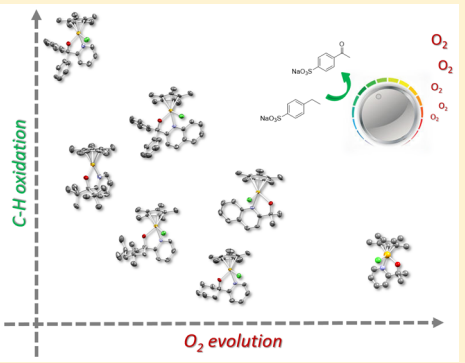

INTRODUCTION

The selective, catalytic oxy-functionalization of inert C−H bonds has long been regarded as one of the holy grails of synthetic chemistry and is an important strategy in the context of sustainable chemistry.[1,2] The main challenges associated with this transformation arise from the strong and nonpolar nature of the C−H bond in combination with issues over control of regio- and chemoselectivity, particularly to prevent over-oxidation. Metal-catalyzed C−H oxidation typically proceeds via one of two routes: insertion of an electrophilic metal center into a C−H bond followed by oxy-functionalization of the metal−alkyl intermediate, or direct insertion of a metal-oxo species into the C−H bond followed by reoxidation of the metal.[2,3] While the topic of C−H activation by metal insertion has been researched extensively,[3] direct C−H oxidation by metal-oxo species is less well explored from an organometallic perspective, despite representing a promising biomimetic strategy. For instance, the active sites in the superbly efficient metallo-enzymes cytochrome P450 and methane monoxygenases are based on Fe-oxo species. A number of synthetic metal-oxo complexes for catalytic C−H activation based on Cr, Mn, Fe, and Ru have been developed for alkene epoxidations and C−H hydroxylations, including the direct conversion of methane to methanol.[4−21]

Recently it has been shown that octahedral half-sandwich iridium(III) complexes can act as effective precatalysts for selectively oxidizing a range of substrates in synthetically useful yields when driven with Ce^{IV} or $NaIO_4$ in aqueous solution.[22,23] Initially developed for chemical energy conversion,[24−28] both C−H and water oxidation reactions are closely related, with interlinked catalytic cycles and common intermediates (Figure 1), as evidenced by water being the source of oxygen in the C−H oxygenation.[29] The formulation of the active species as a closed-shell oxene (most likely d^4 Ir^V)[30] is supported by first-order kinetics in [Ir] for both water[31] and C−H oxidation[23] and retention of configuration in tertiary C−H hydroxylation,[22] observations that argue against the involvement of open-shell oxyl species that would operate via radical rebound[32] and oxo coupling pathways,[24,33] respectively.

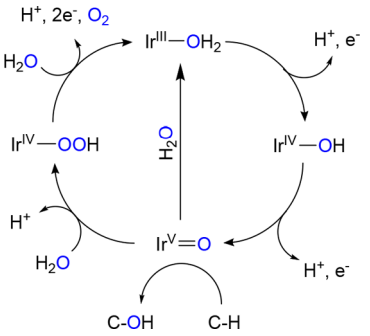

Figure 1. Proposed mechanisms of iridium-catalyzed water (4 electron cycle) and C−H oxidation (two-electron cycle).

In both reactions there is a short induction period during which the Cp*Ir^{III} precursor complexes are oxidatively activated before turnover begins.[34−36] This activation can be performed chemically or electrochemically.[37] It has been shown that the full oxidative activation involves loss of the Cp* ligand[38−40] and results in the formation of a proposed Ir^{IV} μ-oxo dimer (Scheme 1)[36] in which the chelate ligand is retained. The latter

Received: June 29, 2017

© XXXX American Chemical Society

DOI: 10.1021/acs.organomet.7b00492
Organometallics XXXX, XXX, XXX−XXX

Scheme 1. Oxidative Activation of Cp*Ir^{III} Precursors and Formation of Activated Species for Water and C−H Oxidation

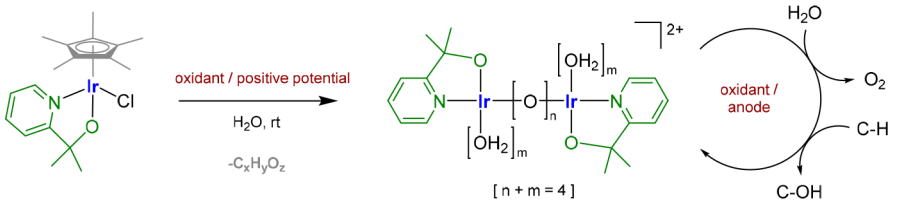

is a crucially important feature in this chemistry, as without an oxidatively robust chelate ligand, polymerization occurs to form IrO_x nanoclusters and particles, which despite being active O_2 evolution catalysts *are inactive in C−H oxidation*.[41] Thus, the further development of these privileged ligands[42] is of great interest in the improvement of these catalysts for application in C−H oxidation, as variation of steric and electronic properties has the potential to increase their scope and utility further.

Here we report the synthesis and characterization of six novel Cp*Ir^{III} precatalysts based on variations of the successful pyridine-alkoxide ligand motif.[42] Spectroscopic analyses reveal strong ligand effects on their oxidative activation and catalytic activity. After pH and solvent environment were optimized, the kinetics of methylene oxidation in para-sulfonated ethylbenzene as model substrate showed a large variation in initial rates and final conversion levels among the catalyst selection, resulting in a molecularly tunable system.

RESULTS AND DISCUSSION

Designing ligands for oxidation catalysts, particularly at the potentials needed for water and C−H oxidation, is challenging as they have to be able to support highly oxidizing metal centers without being degraded themselves.[43] For that reason, many of the traditional organic ligands like carbonyls, olefins, and phosphines that have proven so effective in reductive catalysis are unsuitable for oxidative chemistry.[44] Pyridines, pyrroles, amides, and carboxylates show high oxidative stability when suitably substituted, and whereas primary and secondary alcohols are readily oxidized, tertiary alkoxides are also highly stable. In addition, their π basicity can stabilize high-valent intermediates and enable them to engage in proton management through the oxygen lone pairs.[9]

A range of symmetrically substituted pyalk-type ligands (Figure 2) was synthesized through lithiation of 2-bromopyridine or 2-bromoquinoline followed by reaction with the desired ketone according to previously described methods.[33] This strategy allowed straightforward access to a variety of N^O ligand precursors. Isolated yields of 22−72% were obtained after purification by recrystallization or sublimation (see Supporting Information for details). The alkoxy substituents were varied in terms of steric bulk (methyl, cyclohexyl, ^{t}butyl) and electronics (aliphatic vs aromatic), and the pyridine moiety was extended into a quinoline system. η^2 coordination of the pro-ligands to the Cp*Ir^{III} fragment was achieved by gentle heating with $[Cp^*IrCl_2]_2$ in the presence of a mild inorganic base (Scheme 2).

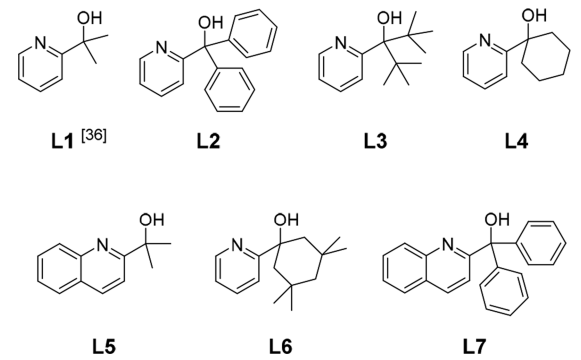

Figure 2. Tertiary 2-pyridine/quinoline alcohols synthesized as proligands for Ir-based oxidation catalysts.

Scheme 2. Synthesis of Cp*Ir^{III} Complexes Using Ligands L1−L7

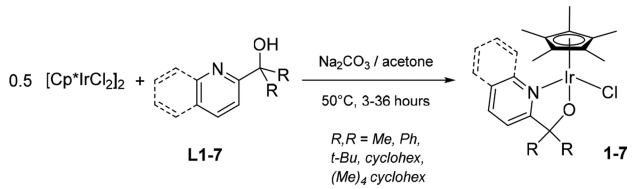

The neutral, monomeric chloro complexes **1**, **2**, **4**−**7** (Figure 3) were obtained in isolated yields of 54−81% after recrystallization.

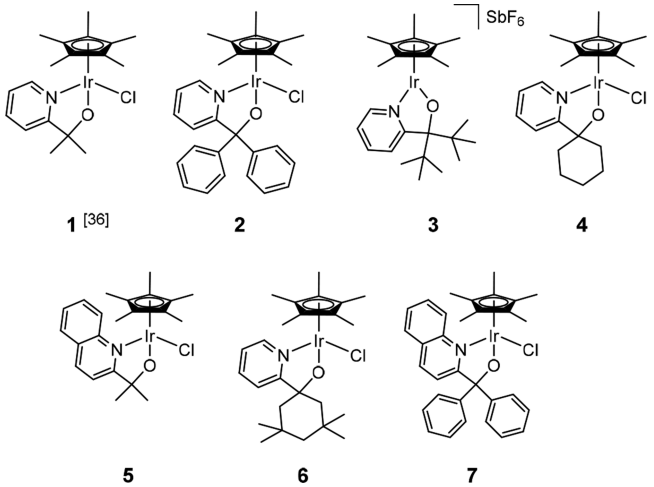

Figure 3. Cp*Ir^{III} complexes **1**−**7** supported by pyalk-type ligands **L1**−**L7** synthesized according to Scheme 2.

Only the bulky bis-^{t}butyl-substituted 2-pyridine alcohol **L3** did not bind to the Cp*Ir^{III} fragment under these conditions, plausibly due to steric clashes between the ^{t}butyl substituents and the Cp* methyl groups in an octahedral complex. Similar steric strain has been observed in related $[Cp^*Ir^{III}(NHC)_2Cl]^+$ complexes with ^{n}butyl substituents on the N-heterocyclic carbenes.[45,46] Addition of MeCN and $AgSbF_6$ to $[Cp^*IrCl_2]_2$ generated $[Cp^*Ir(MeCN)_3][SbF_6]_2$ *in situ*,[47] which is more reactive toward the deprotonated pyalk ligand, and permitted

DOI: 10.1021/acs.organomet.7b00492
Organometallics XXXX, XXX, XXX−XXX

isolation of the cationic 16-electron five-coordinate [Cp*Ir(**L3**)]SbF_6 complex **3**. In this distorted trigonal bipyramidal (dTBP) structure, the pyalk ligand is orthogonal to the plane of the Cp* ligand, thus avoiding steric clash between the alkoxy substituents and the Cp* methyl groups. This coordination mode, involving π donation from the oxygen lone pairs into vacant metal d-orbitals, is well known for various chelating alkoxides[48] and imides[49] and represents a key feature in ligand-assisted bifunctional hydrogenation catalysis.[50]

All new compounds were fully characterized, including single-crystal X-ray diffraction (Figure 4). The solid-state

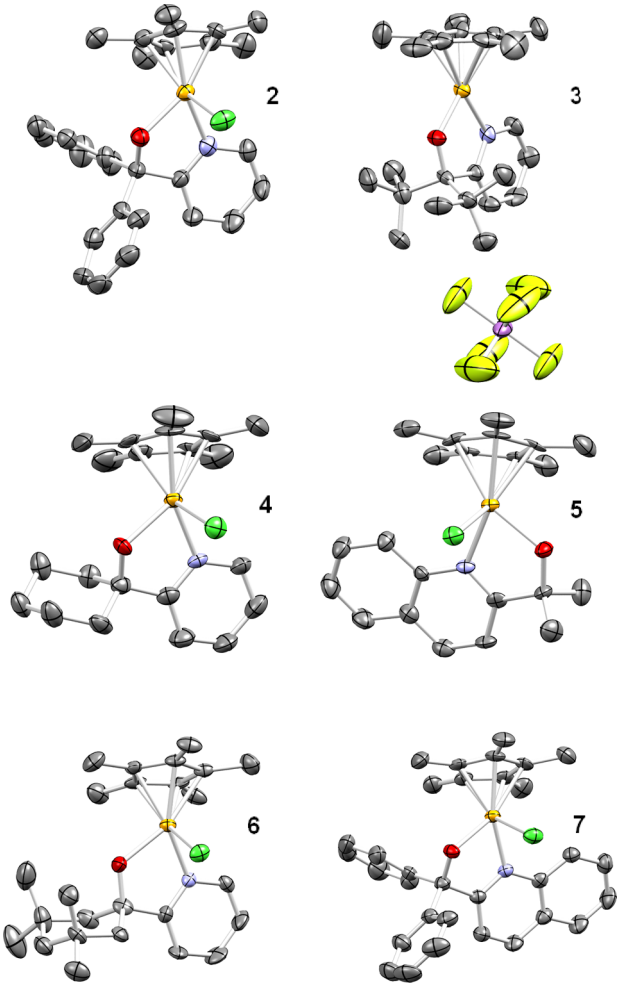

Figure 4. X-ray crystal structures of complexes **2**–**7** (ellipsoids shown at 70% probability level, hydrogen atoms and solvent molecules omitted for clarity; for details see the Experimental Section).

structures confirm the expected geometries with no noticeable distortions; Ir–C distances are 2.16 ± 0.02 Å, Ir–N distances 2.09 ± 0.01 Å, O–Ir–N bond angles 77 ± 1°, and O–Ir–Cl bond angles 86 ± 1.5° in the octahedral complexes. Compounds **1**, **2**, **4**–**7** exhibit Ir–O distances of 2.05 ± 0.01 Å whereas in **3** the Ir–O distance is 1.94 Å, consistent with some double bond character in the cationic five-coordinate complex.[51]

The ability of these N^O ligands to temporarily stabilize a TBP structure via reversible π donation from the oxygen lone pairs (Scheme 3) is also thought to be responsible for the unusually fast ligand exchange kinetics in the octahedral complexes,[52] as evidenced by equivalent ^{1}H NMR signals for

Scheme 3. Reversible π Donation from Oxygen Lone Pairs Facilitating Dissociative Ligand Exchange

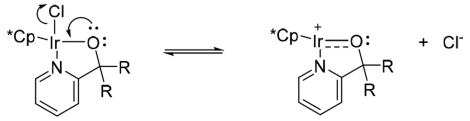

both R groups in complexes **1**–**7** in aqueous methanol at room temperature.

As water coordination is known to be required for these precursors to enter the oxidative activation reaction (Scheme 1),[36] the solution speciation of precursor complexes **1**–**7** in aqueous media can be expected to impact on their rates of activation and catalytic turnover. In addition to intrinsic electronic factors, the ligand bulk, solution pH, and ionic strength can all be expected to influence the equilibria shown in Scheme 4.

To gain some insight into the aqueous solution speciation of **1**–**7**, UV–vis titrations with chloride were carried out (Figure 5). After equilibration between each addition, complexes **1**, **2**, **4**–**7** all showed an increase in absorbance in the region of 350–390 nm with clear isosbestic points with increasing chloride concentration except for **3**, consistent with the observation that an octahedral chloro complex could not be isolated synthetically. These data show that, in the absence of excess halide, the equilibria shown in Scheme 4 lie toward the right, away from the $^{[6]}$Ir-X form for all complexes **1**–**7** under typical reaction conditions (i.e., in aqueous solution at room temperature) and only fully revert to $^{[6]}$Ir-Cl upon the addition of several hundred equivalents of chloride. The distribution of $^{[5]}Ir^+ \leftrightarrow {}^{[6]}Ir\text{-}OH_2^+ \leftrightarrow {}^{[6]}$Ir-OH that prevails without excess chloride is more difficult to assess with certainty and will, in addition to ligand sterics, depend on solution pH. [Attempts at equivalent pH titrations proved inconclusive due to various degrees of degradation of the complexes under basic conditions.] As **3** was not significantly affected by the addition of a large excess of chloride (evidenced by the absence of any isosbestic points), we propose that in neutral aqueous solution all complexes predominantly reside in the sterically most relaxed $^{[5]}Ir^+$ coordination mode, through which they may become available for oxidative activation and catalysis.

The activation reaction of the monomeric Cp^*Ir^{III} complexes with an excess of $NaIO_4$ in aqueous solution, leading to oxidative removal of the Cp* ligand, and formation of the presumed Ir^{IV} μ-oxo dimer (Scheme 1) is typically accompanied by a marked color change from yellow/orange to deep blue. This absorption around 600 nm is characteristic of Ir^{IV}–O–Ir^{IV} linkages and, although also seen in related molecular Ru^{III}–O–Ru^{III} systems,[53] has often been confused with IrO_x formation.[34] Although we have not demonstrated homogeneity for our new derivatives **2**–**7** yet, **1** has been shown to be fully homogeneous over a wide range of conditions using a variety of techniques (including EQCN[54] and DLS[41]), so here we work on the hypothesis that **2**–**7** behave similarly. The oxidative activation reaction according to Scheme 5 was thus followed by time-resolved UV–vis spectroscopy, and markedly different behavior was observed for complexes **1**–**7** reacting with aqueous $NaIO_4$ (Figure 6).

^{1}H NMR analysis showed that in all cases the signal of the bound Cp* ligand had disappeared irreversibly within 1 min after contacting the precursor complexes with the oxidant (Figure S9), with acetate building up as the main Cp*

DOI: 10.1021/acs.organomet.7b00492
Organometallics XXXX, XXX, XXX–XXX

Scheme 4. Solution Equilibria of Cp*Ir^{III} Complexes with Pyalk-Type Complexes in Aqueous Solution[a]

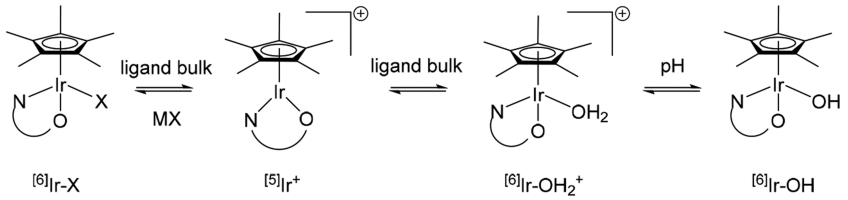

[a]X may be halides from the precursor or added electrolyte.

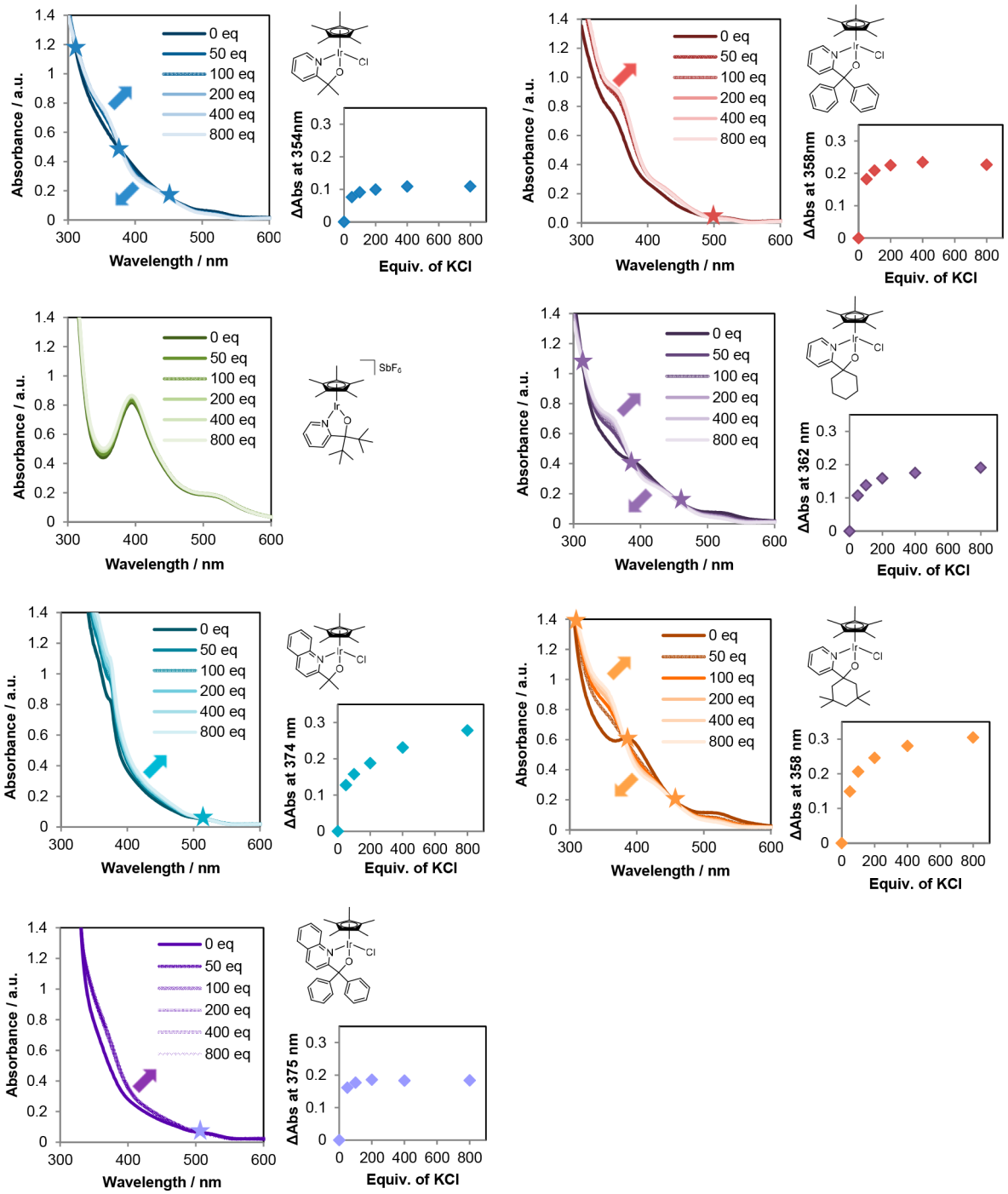

Figure 5. UV−vis titration data of **1**−**7** with KCl at 0.5 mM [Ir] in 4:1 H_2O/^{t}BuOH at room temperature. Isosbestic points are denoted with a star, and the arrows indicate increasing [KCl]. Insets show the change in absorbance calculated for each data set around 370 nm.

DOI: 10.1021/acs.organomet.7b00492
Organometallics XXXX, XXX, XXX−XXX

Scheme 5. Precursor Activation Reaction with Aqueous $NaIO_4$ Followed by UV−Vis Spectroscopy

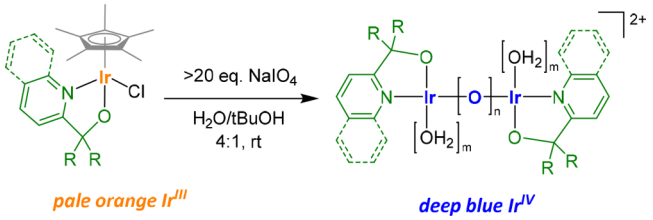

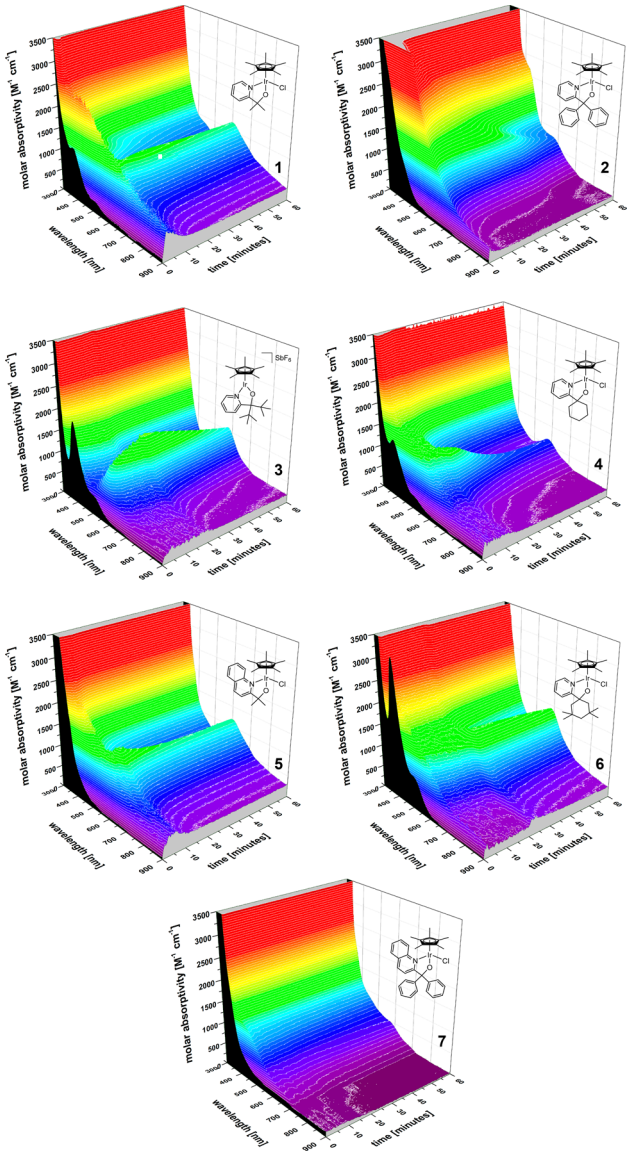

Figure 6. Full-scan UV−vis time course plots (30 s intervals) of the reaction shown in Scheme 5 for compounds **1**−**7** at 0.5 mM [Ir] with 25 mM $NaIO_4$ added after the first scan (black trace) in 4:1 H_2O/^{t}BuOH at room temperature.

degradation product (as previously described for **1**[36]). Thus, any further changes in the UV−vis spectra can be ascribed to further structural transformations leading to the formation of the activated resting state of the catalyst. From Figure 6 and the summary of key parameters in Table 1, it can be seen that under the conditions applied (50 equiv of oxidant) all complexes fully activated within less than 25 min, but with

Table 1. Activation Reaction Times, Absorption Wavelength, and Intensity of the Activated Species from 1−7 with 50 equiv of $NaIO_4$ in 4:1 H_2O/^{t}BuOH

complex	time/min[a]	λ_{max}/nm[b]	ε/M^{-1} cm^{-1} [c]
1	15	599	1354
2	12	567	1308
3	21	579	1366
4	11	572	1400
5	5.5	605	1775
6	22	573	1887
7	2.5	571	594

[a]Time taken to reach maximum absorbance. [b]Wavelength of maximum absorbance. [c]Absorbance at λ_{max}. See also Figures S9 and S10.

varying activation kinetics. The molar absorptivities and λ_{max} in the Ir^{IV}−O−Ir^{IV} regime of the fully activated compounds were similar for **1**−**6**, consistent with a similar species formed in these cases, with the slight differences plausibly reflecting ligand effects on the d(Ir^{IV}) → π*(Ir−O−Ir) transition around 570−610 nm. Interestingly, the activated species possessed different lifetimes. While activated **1**, **5**, and **6** did not show any change over 1 h, **2**, **3**, and **4** began to lose intensity immediately after full activation. Increasing the bulk of the alkoxy substituents in the series of **1** → **4** → **6** → **2** → **3** did not have a major impact on their oxidative activation behavior, even though **3** appeared to be locked in the dTBP structure due to steric pressure in the Cp* precursor. This lends further support to our proposal that all Cp*Ir(pyalk) complexes investigated here prefer the cationic penta-coordinate form in neutral aqueous solution, and shows that these are all available for oxidative activation with periodate. The two cyclohexyl compounds **4** and **6** shared an intermediate phase with maximum absorbance ∼450 nm in their first 10 min, after which similar wavelengths for the activated species were found (572 and 573 nm, respectively). Comparing **1** to **5**, extending the pyridine into a quinoline system, appeared to speed up precursor activation, but not in the case of phenyl substituents. The diphenyl complexes **2** and **7** showed the lowest λ_{max} (567 and 571 nm, respectively), with a persistent shoulder at ∼450 nm which we ascribe to different electronic structures of their activated species (see catalysis results below).

To investigate how these ligand effects translate into catalysis, we compared the behavior of precatalysts **1**−**7** under turnover conditions. Ethyl benzenesulfonate (EBS; Scheme 6) is a convenient model substrate for C−H oxidation

Scheme 6. Selective Oxidation of *p*-ethyl benzenesulfonate

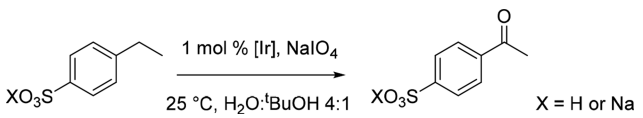

due to its water solubility and diagnostic ^{1}H NMR signals.[23] With iridium-based systems the reaction typically proceeds with clean and selective oxidation of the methylene group to the ketone without aromatic oxygenation—a side reaction often seen with ruthenium-based catalysts and $NaIO_4$.[55]

Although many Cp*Ir^{III} complexes are readily water-soluble, our bulkier derivatives **2**, **3**, and **7** required the addition of an organic cosolvent. In addition, most real-world substrates will be significantly less hydrophilic than the ionic model substrate

DOI: 10.1021/acs.organomet.7b00492
Organometallics XXXX, XXX, XXX−XXX

EBS, hence we tested a variety of oxidation-resistant, water-miscible organic cosolvents in the EBS oxidation according to Scheme 6 utilizing **1** as benchmark. As can be seen from Figure 7, at 20 vol% organic (not to compromise $NaIO_4$ solubility) ^{t}BuOH afforded the best performance, yielding even higher conversions than purely aqueous systems, although initial rates were virtually identical for ^{t}BuOH/H_2O, acetone/H_2O, and pure H_2O. The addition of nitrile and nitro cosolvents appeared to be detrimental to both initial rates and final conversion values, and hexamethylphosphoramide and dimethylamide completely shut down C−H oxidation catalysis, possibly by being oxidized themselves.[56]

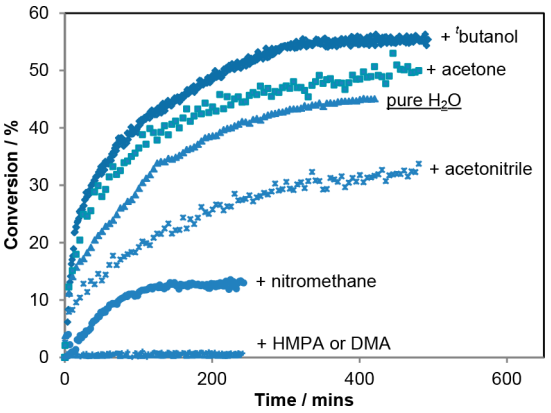

Figure 7. Reaction profiles of the oxidation of EBS (Scheme 6) catalyzed by **1** at 40 mM EBS, 200 mM $NaIO_4$, 0.4 mM (1 mol%) [Ir] at pH 7, 25 °C in various H_2O/cosolvent mixtures (all 4:1 by volume) as derived from *in situ* ^{1}H NMR data.

Moving forward with the optimal ^{t}BuOH/H_2O solvent system, investigation into the effect of solution pH on the reaction showed that neutral pH values gave highest EBS conversions utilizing **1** (Figure 8). This is a potentially complex interplay of varying precursor speciation, oxidant potential, active catalyst speciation and stability, and possibly electronic effects on the ionic substrate, though whatever the exact cause, the observation that very low C−H oxidation conversions are obtained under either acidic or basic conditions is important information for practical application.

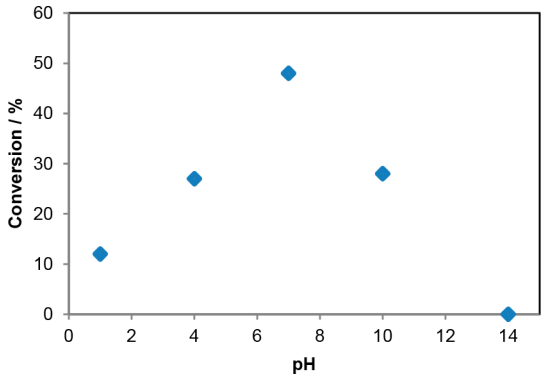

Figure 8. Conversion values of the oxidation of EBS (Scheme 6) catalyzed by **1** at 40 mM EBS, 200 mM $NaIO_4$, 0.4 mM (1 mol%) [Ir], 25 °C in 4:1 H_2O/^{t}BuOH after 10 min reaction time (pH adjusted with HNO_3/NaOH).

Comparing EBS oxidation reaction profiles from *in situ* ^{1}H NMR utilizing **1**−**7** under optimized conditions showed markedly different catalytic performance (Figure 9). No conversion occurred without any iridium added, but all catalysts were active in the reaction shown in Scheme 6 with 100% selectivity to the para-sulfonated acetophenone product, though greatly varying in initial rates and final conversion values. Table 2 summarizes key performance data under the conditions applied.

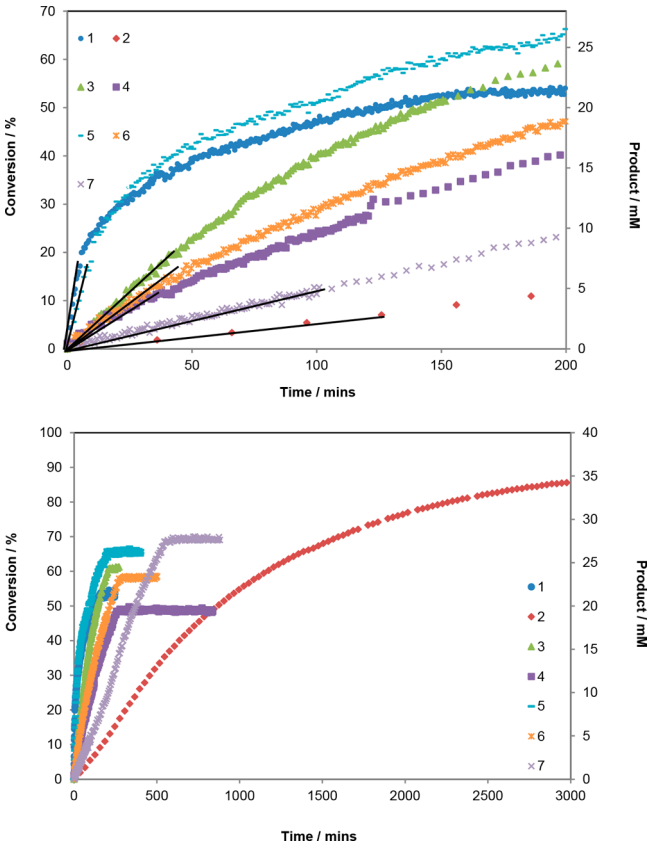

Figure 9. Initial (top) and full (bottom) ^{1}H NMR time course data of the oxidation of EBS (Scheme 6) with complexes **1**−**7** at 40 mM EBS, 200 mM $NaIO_4$, 0.4 mM (1 mol%) [Ir] at pH 7, 25 °C in 4:1 H_2O/^{t}BuOH. Initial rates shown as black lines.

The dimethyl-substituted complexes **1** and **5** displayed by far the fastest initial rates, and the diphenyl complexes **2** and **7**

Table 2. Initial Rates, Final Conversion Values, and Time Taken to Final Conversion of the Reaction Profiles Shown in Figure 9

precatalyst	initial k_{obs}/mM min^{-1} [a]	catalyst TOF/h^{-1} [b]	conversion plateau/% [c]	time to plateau/h
1	1.61	242	55	2.6
2	0.03	4	88	60
3	0.19	29	65	3.3
4	0.13	20	52	4.3
5	0.99	149	68	3.2
6	0.14	21	60	4.5
7	0.05	8	70	9.0

[a]Calculated from initial gradient of product concentration over time (linear regime; see Figure 9). [b]Initial reaction rate divided by catalyst concentration. [c]Averaged value over plateau.

DOI: 10.1021/acs.organomet.7b00492
Organometallics XXXX, XXX, XXX−XXX

were slowest. The bulkier alkyl-substituted complexes **3**, **4**, and **6** gave intermediate results closer to those obtained with the diphenyl complexes. This trend roughly mirrors the one seen in the precursor activation reaction (Table 1). However, as all complexes were fully activated within 25 min at much lower oxidant loadings (50 equiv in the UV−vis experiments compared to 500 equiv used for catalysis), and none of the C−H oxidation reaction profiles showed sigmoidal kinetics indicative of limiting precursor activation, we conclude that these varying rates reflect intrinsic differences of the fully activated catalysts originating from the various pyalk ligands. Even in case of **2**, the rate did not accelerate over the 60 h reaction time, suggesting that the precursor complex did activate but, in line with its slightly different UV−vis signature (cf. Figure 6), formed a distinct active species.

When the full reaction profile is considered (Figure 9, bottom), it can be seen that the reaction conversions plateaued at different levels for the different precatalysts (Table 2), although a 5-fold excess of oxidant over substrate was used in all cases. To test whether catalyst deactivation was responsible for the limited conversion values, a second portion of oxidant was added to a catalytic run with **5** after conversion had stalled after 3.5 h. As shown in Figure 10, catalysis immediately

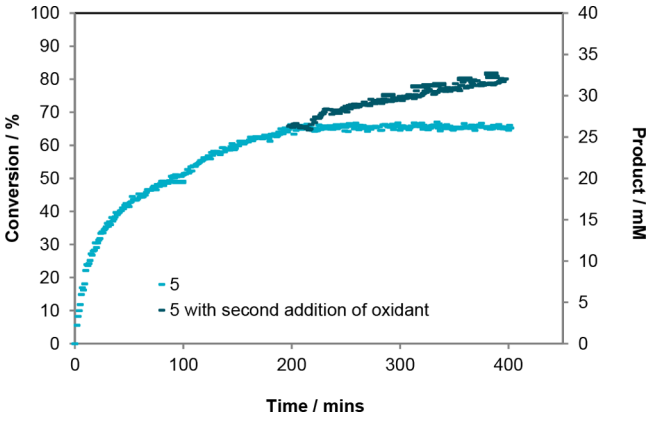

Figure 10. ^{1}H NMR time course of the oxidation of EBS (Scheme 6) with complex **5** with a second addition of $NaIO_4$ at 40 mM EBS, 200 mM $NaIO_4$ (initial), 0.4 mM (1 mol%) [Ir] at pH 7, 25 °C in 4:1 H_2O/^{t}BuOH.

resumed with a stable rate, nicely extrapolating the initial reaction profile, proving that the catalyst remained active. We therefore ascribe the conversion plateaus to the system becoming depleted of oxidant, and with the amount not seen in C−H oxidation product being consumed in the parallel oxygen evolution reaction. These different C−H oxidation plateaus are thus indicative of the individual C−H vs O−H oxidation selectivity (i.e., a branching ratio).

The fact that the branching ratios of water vs C−H oxidation appear to be directly influenced by the N^O ligand in the precursor is exciting in that it indicates that there is scope for molecular control over these highly oxidizing catalyst systems based on ligand design. The branching ratio being a pure selectivity measure during turnover (cf. Scheme 1) only reflects intrinsic differences of the fully activated species with no interference from ligand effects on precursor speciation and activation. In this respect the slowest but most C−H selective precatalyst **2** is interesting, as the phenyl substitution pattern appears to impart C−H over O−H preference onto the catalyst.

In order to quantify the amount of O_2 generated during EBS oxidation with precatalysts **1**−**7**, oxygen assays using a Clarke-type electrode were undertaken under the same reaction conditions (Figure 11). All complexes except **2** showed some

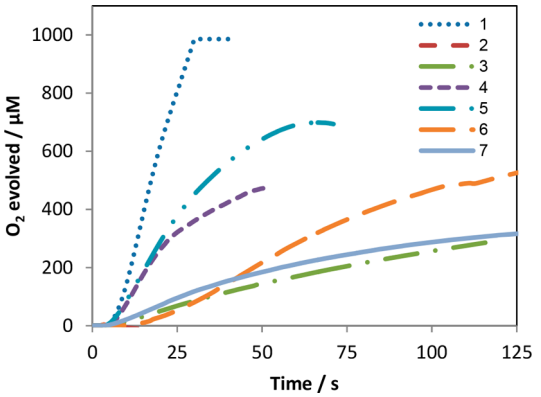

Figure 11. Oxygen evolution traces of the precatalysts **1**−**7** during C−H oxidation catalysis at 40 mM EBS, 200 mM $NaIO_4$, 0.4 mM (1 mol %) [Ir] at pH 7, 25 °C in 4:1 H_2O/^{t}BuOH using a calibrated Clark electrode.

O_2 generation activity during EBS oxidation, fully in line with its highest C−H oxidation efficiency observed with EBS (Figure 9 and Table 2). The relative order in activity for O_2 evolution was similar to that seen in catalytic EBS oxidation, with **1** being the most active precursor, followed by **5**, and then **3**, **6**, **7**, and **2** (Table 3).

Table 3. Activation Times and Initial Rates of the O_2 Evolution Profiles Shown in Figure 11

precatalyst	activation time/s[a]	initial k_{obs}/mM min^{-1} [b]	catalyst TOF/h^{-1} [c]
1	5	2.98	448
2	n.a.	0	0
3	6	0.21	32
4	4	0.89	134
5	3	1.26	188
6	9	0.25	38
7	3	0.28	43

[a]Lag phase between precatalyst addition and onset of O_2 evolution. [b]Calculated from initial gradient of product concentration over time (average from triplicates). [c]Initial reaction rate divided by catalyst concentration.

Activation periods were shortened to a few seconds for all precatalysts under the conditions applied (500 equiv of $NaIO_4$ per Ir), with the same reactivity order as in the UV−vis experiments (Figure 6 and Table 1). Initial O_2 evolution rates were in the same order of magnitude as C−H oxidation rates (Table 2), but O_2 evolution occurred on a faster time scale and ceased after 2−3 min. Due to the much higher water than EBS concentrations the two competing oxidation reactions thus occurred sequentially once precursor activation was complete. The thermodynamically more challenging substrate (water) only got oxidized in early stages of the reaction where higher solution potentials existed, with C−H oxidation occurring once oxidant concentration had been depleted sufficiently for it to compete with the harder to oxidize but more abundant substrate water. Plotting initial O_2 evolution rates versus C−H

DOI: 10.1021/acs.organomet.7b00492
Organometallics XXXX, XXX, XXX−XXX

oxidation efficiency (Figure 12) suggests this competition to be a measure of the oxidizing power of the activated catalyst. With

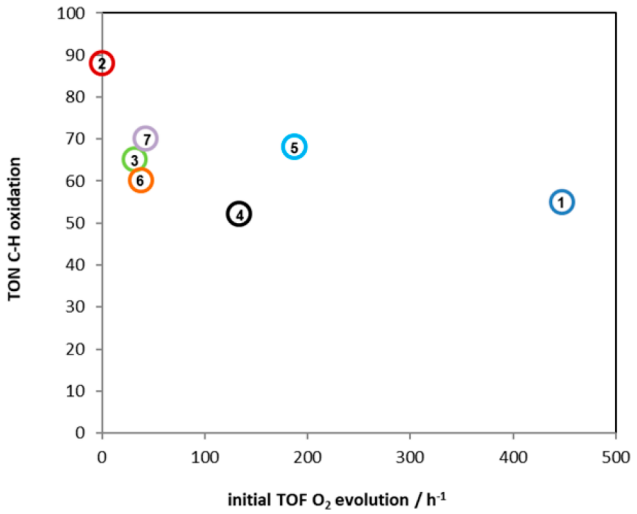

Figure 12. Correlation of initial O_2 evolution rates with final EBS oxidation yields catalyzed by **1**−**7** (40 mM EBS, 200 mM $NaIO_4$, 0.4 mM (1 mol%) [Ir] at pH 7, 25 °C in 4:1 H_2O/^{t}BuOH).

this view, the higher C−H oxidation efficiency of **2** can be rationalized; the electron-withdrawing aryl substituents result in a less oxidizing active species which does not evolve any O_2 but slowly turns over nearly all of the C−H substrate present.

Although no global correlation exists for the limited sample size of **1**−**7**, an activity analysis with respect to ligand effects does reveal some interesting trends:

(a) Extending the pyridine into a quinoline, with alkyl alkoxide substituents (**1** → **5**), decreases the rate and increases the C−H selectivity.
(b) Increasing the bulk of the alkoxide substituents (**1** → **4**, **6**, **3**) greatly decreases the rate and slightly increases C−H selectivity.
(c) Substituting alkyl with aryl alkoxide substituents greatly reduces the rate (**1** → **2**) and significantly improves C−H selectivity, though not with a quinoline backbone (**2** → **7**).

Thus, if rate is most important, a pyalk ligand with minimum steric demand and high donor power should be used, whereas fine-tuning of the electronics via modification of electron-withdrawing aryl substituents may yield slower but more C−H selective oxidation catalysts.

CONCLUSIONS

We have described the syntheses, solid-state and solution structures, and catalytic properties of six new Cp* Ir^{III} complexes with various symmetrically substituted pyridine-alkoxide ligands, precursors to potent oxidation catalysts. The steric bulk of the alkoxide substituents impacts on the coordination mode of the ligand through clashes with the Cp* ligand in the octahedral form. However, all chloride complexes have been shown to readily ionize and, in neutral aqueous solution, appear to prefer cationic penta-coordination of the metal from which they are available for oxidative activation with aqueous $NaIO_4$. Although their individual activation kinetics vary, there is no indication for limiting precatalytic ligand effects within the series of **1**−**7**. We have shown the importance of the reaction environment on their catalytic performance and identified ^{t}BuOH as the most beneficial organic cosolvent for aqueous C−H oxidation at neutral pH for these iridium catalysts. Kinetic profiling of the catalytic oxidation of EBS with $NaIO_4$ showed that the investigated catalysts plateau at different conversions when becoming depleted of oxidant but are stable and can be reactivated by repeated addition of oxidant to reach higher turnover numbers. Monitoring O_2 evolution during C−H oxidation catalysis showed the two reactions to occur sequentially, with more active catalysts generating more O_2 before the slower C−H oxidation catalysis set in. The various pyalk-type ligands synthesized (**L2**−**L7**) not only impact on the precursor activation reaction but also modulate the activity and thereby the selectivity of the active species. Thus, for the first time, molecular control over these highly oxidizing iridium catalysts has been demonstrated, a finding that opens the door to further improvement of these promising catalysts based on ligand engineering.

EXPERIMENTAL SECTION

General. Organic solvents were purified by passing over activated alumina with dry argon. All chemicals were purchased from major commercial suppliers and used as received. Syntheses were performed under an inert atmosphere of dry argon using standard Schlenk techniques. NMR spectra were recorded on either 400 or 500 MHz Bruker Avance spectrometers and referenced to residual protio-solvent signals. The chemical shift δ is reported in units of parts per million (ppm). Elemental analyses were provided by the Science Centre of London Metropolitan University, and mass spectrometry (MS) was performed by the EPSRC UK National Mass Spectrometry Facility at Swansea University. Details of the single-crystal X-ray data collections and ligand syntheses can be found in the Supporting Information.

[Cp*IrCl$_2$]$_2$.[26] $IrCl_3 \cdot 3H_2O$ (2.84 mmol, 1.00 g) was added to a 20 mL microwave flask with methanol (10 mL) and water (1 mL). The solution was degassed by bubbling with argon with stirring for 5 min. Under a continuous stream of argon, pentamethylcyclopentadiene (3.67 mmol, 0.5 g) was added and the mixture was stirred for a further 2 min. The flask was sealed, put into a microwave reactor and heated to 140 °C for 20 min. The reaction was quenched with ice and a red/orange precipitate formed. The mixture was filtered under vacuum using a fritted funnel, and the solid residue extracted with dichloromethane (20 mL). The product was recrystallized from DCM (3 mL) by addition of Et_2O (20 mL). Removal of the supernatant and drying *in vacuo* yielded a microcrystalline red/orange powder. Yield: 686 mg (61%). ^{1}H NMR (400 MHz, $CDCl_3$): δ = 1.57 (s, 15H, $[CH_3]_5$).

[η^5(C$_5$Me$_5$)Ir^{III}\{2-(2-pyridyl)-2-propanolate-κO,κN\}Cl], 1.[54] $[Cp^*IrCl_2]_2$ (0.1 mmol, 79.8 mg), dimethyl(2-pyridyl)methanol (0.2 mmol, 27.4 mg), and Na_2CO_3 (0.8 mmol, 84.8 mg) were dissolved in acetone (15 mL). The resulting orange solution was stirred for 6 h at 50 °C, after which time the solution had turned yellow. $MgSO_4$ was added, and after stirring for 10 min the solution was filtered and the solvent removed *in vacuo* to afford an orange-red solid. The product was recrystallized from DCM by the addition of diethyl ether (5 mL). The yellow supernatant was removed and the powder dried *in vacuo* to give yellow-orange microcrystals. Yield: 0.036 g (72%). ^{1}H NMR (400 MHz, $CDCl_3$): δ = 8.53 (d, J = 5.7 Hz, 1H, H_{arom}), 7.66 (t, J = 7.8 Hz, 1H, H_{arom}), 7.14 (m, 2H, H_{arom}), 1.69 (s, 15H, $[CH_3]_5$), 1.53 (s, 6H, $[CH_3]_2$).

[η^5(C$_5$Me$_5$)Ir^{III}\{diphenyl(2-pyridyl)methanolate-κO,κN\}Cl], 2. $[Cp^*IrCl_2]_2$ (0.089 mmol, 70.0 mg), diphenyl(2-pyridyl)methanol (0.194 mmol, 50.7 mg), and Na_2CO_3 (0.704 mmol, 74.6 mg) were dissolved in acetone (20 mL). The resulting orange solution was stirred for 4 h at 50 °C, after which time the solution had turned yellow. $MgSO_4$ was added, and after stirring for 10 min the solution was filtered and the solvent removed *in vacuo* to afford a yellow oil.

DOI: 10.1021/acs.organomet.7b00492
Organometallics XXXX, XXX, XXX−XXX

The product was washed with diethyl ether (2 × 5 mL). The yellow supernatant was removed and the powder dried *in vacuo* to give an orange-yellow powder. Single crystals suitable for X-ray diffraction analysis were grown by solvent evaporation ($CDCl_3$) at room temperature. Yield: 0.0447 g (81%). ^{1}H NMR (400 MHz, $CDCl_3$): δ = 8.63 (d, J = 5.7 Hz, 1H, H_{arom}), 7.56 (t, J = 7.7 Hz, 1H, H_{arom}), 7.25 (s, 20H, H_{arom} + CH_{phenyl}), 6.82 (d, J = 7.9 Hz, 1H, H_{arom}), 1.40 (s, 15H, $[CH_3]_5$); ^{13}C NMR (100 MHz, $CDCl_3$): δ = 173.2 (C_{arom}), 150.1 ($CH_{pyridine}$), 136.2 ($CH_{pyridine}$), 129.6 (CH_{phenyl}), 128.3 (CH_{phenyl}), 127.6 (CH_{phenyl}), 126.8 (CH_{phenyl}), 125.7 (CH_{phenyl}), 124.0 (CH_{phenyl}), 94.6 (C), 84.3 (C_{Cp^*}), 8.8 ($CH_{3\ Cp^*}$); HR ESI-MS (+): m/z calculated for $C_{28}H_{29}ClIrNO$, $[M - H]^+$ 622.1476, 620.1460; found 622.1474, 620.1455; $[M - Cl]^+$ 588.1873, 586.1850; found 588.1866, 586.1848. Elemental analysis: calcd (%) for $C_{28}H_{29}ClIrNO$: C 53.96, H 4.69, N 2.25; found: C 53.96, H 4.74, N 2.34. Crystal data [CCDC no. 1413039]: $C_{30}H_{31}Cl_7IrNO$ (Ir2 + 2 $CHCl_3$), M = 861.91, monoclinic, $P2_1/n$, a = 12.3236(2) Å, b = 16.4094(3) Å, c = 16.4100(3) Å, β = 92.2863(11)°, V = 3315.84(10) Å^3, Z = 4, d_{calc} = 1.727 g/cm^3, T = 150 K, 66 209 reflections collected, 7585 independent reflections (R_{int} = 0.1312), final R_1 = 0.0422, final wR_2 = 0.0898, GoF = 1.010.

[η^5(C_5Me_5)Ir^{III}\{2,2,4,4-tetramethyl-3-(2-pyridyl)-3-pentanolate-κO,κN\}] hexafluoroantimonate, 3. $[Cp^*IrCl_2]_2$ (0.1 mmol, 79.8 mg), 2,2,4,4-tetramethyl-3-(2-pyridyl)-3-pentanol, (0.22 mmol, 48.7 mg), and Na_2CO_3 (0.8 mmol, 84.8 mg) were dissolved in acetone (20 mL). The resulting orange solution was stirred for 20 h at 50 °C, without observing any color changes. $AgSbF_6$ (0.22 mmol, 0.0756 g) and acetonitrile were therefore added (2 mL), and the mixture stirred for a further 23 h, after which time the solution had turned yellow and a fine, colorless solid was observed. The solution was filtered through a 0.2 μm Teflon syringe filter and the solvent removed *in vacuo*. The resulting red-brown residue was dissolved in dichloromethane (2 mL) and diethyl ether (30 mL) added, causing the precipitation of a red solid. The supernatant was removed and the product dried to afford a fine dark red powder. Single crystals suitable for X-ray diffraction analysis were grown by diffusion of hexane into a DCM solution at room temperature. Yield: 0.036 g (46%). ^{1}H NMR (400 MHz, $CDCl_3$): δ = 9.15 (d, J = 5.9 Hz, 1H, H_{arom}), 8.00 (d, J = 8.26 Hz, 1H, H_{arom}), 7.91 (t, J = 7.4 Hz, 1H, H_{arom}), 7.65 (t, J = 6.7 Hz, 1H, H_{arom}), 1.88 (s, 15H, $[CH_3]_5$), 1.90 (s, 18H, $[CH_3]_6$); ^{13}C NMR (100 MHz, $CDCl_3$): δ = 178.2 ($C_{pyridine}$), 152.4 ($CH_{pyridine}$), 138.0 ($CH_{pyridine}$), 125.4 ($CH_{pyridine}$), 123.4 ($CH_{pyridine}$), 103.9 (C), 88.9 (C_{Cp^*}), 41.2 ($C_{t\text{-butyl}}$), 28.9 ($CH_{3\ t\text{-butyl}}$), 9.8 ($CH_{3\ Cp^*}$); ESI-MS (+): m/z calculated for $C_{27}H_{45}F_6IrNOSb$, $[M - SbF_6]^+$, 548.2500, 546.2476; found 548.2493, 546.2472. Elemental analysis: calcd (%) for $C_{27}H_{45}F_6IrNOSb$: C 36.79, H 4.76, N 1.79, found: C 36.70, H 4.83, N 1.77. Crystal data [CCDC no. 1413040]: $C_{24}H_{37}F_6IrNOSb$ (**3**), M = 783.49, triclinic, $P\bar{1}$, a = 10.9884(2) Å, b = 11.9229(2) Å, c = 12.9393(2) Å, α = 113.6957(8)°, β = 114.4785(7)°, γ = 91.0354(7)°, V = 1377.69(4) Å^3, Z = 2, d_{calc} = 1.889 g/cm^3, T = 150 K, 25 636 reflections collected, 7937 independent reflections (R_{int} = 0.1343), final R_1 = 0.0710, final wR_2 = 0.1787, GoF = 1.014.

[η^5(C_5Me_5)Ir^{III}\{1-(2-pyridyl)cyclohexanolate-κO,κN\}Cl], 4. $[Cp^*IrCl_2]_2$ (0.2 mmol, 160 mg), 1-(2-pyridyl)cyclohexanol (0.3 mmol, 62.0 mg), and Na_2CO_3 (0.8 mmol, 84.8 g) were dissolved in acetone (20 mL). The resulting orange solution was stirred for 5 h at 50 °C, after which time the solution had turned yellow. $MgSO_4$ was added, and after stirring for 10 min the solution was filtered and the solvent removed *in vacuo* to afford an orange-yellow oil. The product was washed with diethyl ether (20 mL). The yellow supernatant was removed and the powder dried *in vacuo* to give an orange powder. Single crystals suitable for X-ray diffraction analysis were grown by diffusion of hexane into a DCM solution at room temperature. Yield: 0.0581 g (54%). ^{1}H NMR (400 MHz, $CDCl_3$): δ = 8.49 (d, J = 5.1 Hz, 1H, H_{arom}), 7.63 (t, J = 7.9 Hz, 1H, H_{arom}), 7.12 (m, 2H, H_{arom}), 1.66 (s, 15H, $[CH_3]_5$) 2.06 (m, 2H, CH_{hexyl}), 1.81 (m, 1H, CH_{hexyl}), 1.52 (m, 3H, CH_{hexyl}), 1.38 (m, 2H, CH_{hexyl}), 1.17 (m, 2H, CH_{hexyl}); ^{13}C NMR (100 MHz, $CDCl_3$): δ = 178.2 ($C_{pyridine}$), 149.7 ($CH_{pyridine}$), 137.1 ($CH_{pyridine}$), 123.5 ($CH_{pyridine}$), 122.2 ($CH_{pyridine}$), 84.6 (C), 83.9 (C_{Cp^*}), 40.9 (CH_2), 26.3 (CH_2), 22.1 (CH_2), 9.1 ($CH_{3\ Cp^*}$); ESI-MS (+): m/z calculated for $C_{21}H_{30}ClIrNO$, $[M + H]^+$, 540.1632, 538.1616; found 540.1626, 538.1609; $[M - Cl]^+$, 504.1878, 502.1855; found 504.1865, 502.1845. Elemental analysis: calcd (%) for $C_{21}H_{30}ClIrNO$: C 46.78, H 5.42, N 2.60; found: C 46.69, H 5.41, N 2.6. Crystal data [CCDC no. 1413041]: $C_{21}H_{31}ClIrNO_2$ (**4** + H_2O), M = 557.12, monoclinic, $P2_1/c$, a = 17.3755(4) Å, b = 15.3635(3) Å, c = 15.7991(3) Å, β = 90.789(2)°, V = 4217.15(15) Å^3, Z = 8, d_{calc} = 1.755 g/cm^3, T = 150 K, 18 642 reflections collected, 18 642 independent reflections (R_{int} = 0.0513), final R_1 = 0.0559, final wR_2 = 0.1496, GoF = 1.056.

[η^5(C_5Me_5)Ir^{III}\{2-(2-quinolyl)-2-propanolate-κO,κN\}Cl], 5. $[Cp^*IrCl_2]_2$ (0.214 mmol, 165 mg), 2-(2-quinolyl)-2-propanol (0.6 mmol, 127 mg), and Na_2CO_3 (1.8 mmol, 190 mg) were dissolved in acetone (20 mL). The resulting orange solution was stirred for 3.5 h at 50 °C, after which time the solution had turned yellow. $MgSO_4$ was added, and after stirring for 10 min the solution was filtered and the solvent removed *in vacuo* to afford a brown oil. The product dissolved in DCM (5 mL), and hexane was added (25 mL). Upon storage at −20 °C a precipitate formed. The clear orange supernatant was removed and the solid dried *in vacuo* to give a dark orange powder. Single crystals suitable for X-ray diffraction analysis were grown by solvent evaporation (DCM) at room temperature. Yield: 78.9 mg (68%). ^{1}H NMR (400 MHz, $CDCl_3$): δ = 8.51 (d, J = 8.2 Hz, 1H, H_{arom}), 8.09 (d, J = 8.7 Hz, 1H, H_{arom}), 7.80 (d, J = 7.9 Hz, 1H, H_{arom}), 7.78 (t, J = 7.8 Hz, 1H, H_{arom}), 7.56 (t, J = 7.7 Hz, 1H, H_{arom}), 7.19 (d, J = 8.5 Hz, 1H, H_{arom}), 1.61 (s, 21H, $[CCH_3]_5$ + $[CH_3]_2$); ^{13}C NMR (100 MHz, $CDCl_3$): δ = 179.7 ($C_{quinoline}$), 144.6 ($C_{quinoline}$) 137.2 ($CH_{quinoline}$), 132.8 ($CH_{quinoline}$), 130.5 ($CH_{quinoline}$), 128.6 ($C_{quinoline}$), 127.7 ($CH_{quinoline}$), 127.0 ($CH_{quinoline}$), 119.2 ($CH_{quinoline}$), 86.6 (C), 84.4 (C_{Cp^*}), 35.2 (CH_3), 33.1 (CH_3), 9.4 ($CH_{3\ Cp^*}$); ESI-MS (+): m/z calculated for $C_{22}H_{27}ClIrNO$, $[M + H]^+$, 550.1475, 548.1460; found 550.1470, 548.1453; $[M - Cl]^+$, 514.1722, 512.1699; found 514.1710, 512.1689. Elemental analysis: calcd (%) for $C_{22}H_{27}ClIrNO$: C 48.12, H 4.96, N 2.55, found: C 47.89, H 4.96, N 2.59. Crystal data [CCDC no. 1413043]: $C_{22}H_{29}ClIrNO_2$ (**5** + H_2O), M = 567.11, monoclinic, $P2_1$, a = 7.8422(3) Å, b = 13.7658(4) Å, c = 10.3658(4) Å, β = 106.632(4)°, V = 1072.22(7) Å^3, Z = 2, d_{calc} = 1.757 g/cm^3, T = 150 K, 12 281 reflections collected, 4980 independent reflections (R_{int} = 0.0407), final R_1 = 0.0277, final wR_2 = 0.0465, GoF = 1.000.

[η^5(C_5Me_5)Ir^{III}\{3,3,5,5-tetramethyl-1-(2-pyridyl)-cyclohexanolate-κO,κN\}Cl], 6. $[Cp^*IrCl_2]_2$ (0.1 mmol, 79.3 mg), 3,3,5,5-tetramethyl-1-(2-pyridyl)cyclohexanol (0.24 mmol, 58.3 mg) and Na_2CO_3 (0.8 mmol, 84.8 g) were dissolved in acetone (15 mL). The resulting orange solution was stirred at 50 °C for 36 h, after which time the solution had turned yellow. $MgSO_4$ was added, and after stirring for 10 min the solution was filtered and the solvent removed *in vacuo* to afford a brown oil. The product recrystallized from DCM (1 mL) upon addition of diethyl ether (20 mL) to give a light brown powder. Single crystals suitable for X-ray diffraction analysis were grown by solvent evaporation (DCM) at room temperature. Yield: 0.0455 mg (76%). ^{1}H NMR (400 MHz, $CDCl_3$): δ = 8.51 (d, J = 5.2 Hz, 1H, H_{arom}), 7.59 (t, J = 8.0 Hz, 1H, H_{arom}), 7.08 (m, 2H, H_{arom}), 1.83 (m, 6H, $H_{cyclohexyl}$), 1.67 (s, 15H, $[CCH_3]_5$), 1.45 (s, 6H, $[CH_3]_2$), 0.87 (s, 6H, $[CH_3]_2$); ^{13}C NMR (100 MHz, $CDCl_3$): δ = 181.6 ($C_{pyridine}$), 148.9 ($CH_{pyridine}$), 136.2 ($CH_{pyridine}$), 123.1 ($CH_{pyridine}$), 122.7 ($CH_{pyridine}$), 89.1 (C), 83.3 (C_{Cp^*}), 53.3 (CH_2), 52.8 (CH_2), 36.9 (CH_3), 31.9 (C), 29.1 (CH_3), 8.7 ($CH_{3\ Cp^*}$); ESI-MS (+): m/z calculated for $C_{25}H_{37}ClIrNO$, $[M - Cl]^+$, 558.2476, 560.2500; found 558.2484, 560.2501. Elemental analysis: calcd (%) for $C_{25}H_{37}ClIrNO$: C 50.45, H 6.27, N 2.35; found: C 50.41, H 6.14, N, 2.42. Crystal data [CCDC no. 1413044]: $C_{25}H_{37}ClIrNO$ (**6**), M = 595.20, monoclinic, $P2_1/c$, a = 16.6537(5) Å, b = 16.6270(10) Å, c = 9.0691(5) Å, β = 96.446(4)°, V = 2495.4(2) Å^3, Z = 4, d_{calc} = 1.584 g/cm^3, T = 150 K, 10 408 reflections collected, 5604 independent reflections (R_{int} = 0.0458), final R_1 = 0.0411, final wR_2 = 0.0527, GoF = 0.980.

[η^5(C_5Me_5)Ir^{III}\{diphenyl(2-quinolyl)methanolate-κO,κN\}Cl], 7. $[Cp^*IrCl_2]_2$ (0.1 mmol, 79.3 mg), diphenyl(2-quinolyl)methanol (0.24 mmol, 74.7 mg), and Na_2CO_3 (0.8 mmol, 84.8 mg) were dissolved in acetone (15 mL). The resulting orange solution was

DOI: 10.1021/acs.organomet.7b00492
Organometallics XXXX, XXX, XXX−XXX

stirred at 50 °C for 36 h, after which time the solution had turned yellow. $MgSO_4$ was added, and after stirring for 10 min the solution was filtered and the solvent removed *in vacuo* to afford an orange oil. The product was dissolved in DCM (1 mL), and diethyl ether was added (20 mL). Upon storage at −20 °C a precipitate formed. The supernatant was removed and the solid dried *in vacuo* to give an orange powder. Single crystals suitable for X-ray diffraction analysis were grown by solvent evaporation (toluene) at room temperature. Yield: 0.0501 mg (74%). ^{1}H NMR (400 MHz, $CDCl_3$): δ = 8.63 (d, J = 8.8 Hz, 1H, H_{arom}), 7.96 (d, J = 8.8 Hz, 1H, H_{arom}), 7.79 (m, 2H, H_{arom}), 7.60 (t, J = 7.8 Hz, 1H, H_{arom}), 7.48 (d, J = 8.0 Hz, 2H, H_{phenyl}), 7.40 (d, J = 8.0 Hz, 2H, H_{phenyl}), 7.32 (m, 3H, H_{phenyl}), 7.14 (m, 3H, H_{phenyl}), 6.98 (d, J = 8.4 Hz, 1H, H_{arom}), 1.61 (s, 15H, $[CH_3]_5$); ^{13}C NMR (100 MHz, $CDCl_3$): δ = 174.9 ($C_{quinoline}$), 151.8 (C_{arom}), 150.0 (C_{arom}), 144.5 (C_{arom}), 135.6 (CH_{arom}), 132.8 (CH_{arom}), 130.5 (CH_{arom}), 129.7 (CH_{arom}), 128.8 (CH_{arom}), 127.9 (CH_{arom}), 127.6 (CH_{arom}), 127.4 (CH_{arom}), 127.1 (CH_{arom}), 126.6 (CH_{arom}), 123.4 (CH_{arom}), 97.1 (C), 84.7 (C_{Cp*}), 9.2 ($CH_{3\ Cp*}$); ESI-MS (+): m/z calculated for $C_{32}H_{31}ClIrNO$, $[M - Cl]^+$, 636.2006, 638.2031; found 636.2009, 638.2025. Elemental analysis: calcd (%) for $C_{32}H_{31}ClIrNO$: C 57.09, H 4.64, N 2.08; found: C 57.18, H 4.49, N 2.23. Crystal data [CCDC no. 1413042]: $C_{71}H_{70}Cl_2Ir_2N_2O_2$ (7 + 0.5 toluene), M = 1438.59, monoclinic, $P2_1/c$, a = 20.7893(4) Å, b = 9.41350(10) Å, c = 15.8988(3) Å, β = 109.826(2)°, V = 2926.97(9) Å^3, Z = 2, d_{calc} = 1.632 g/cm^3, T = 150 K, 21 626 reflections collected, 6988 independent reflections (R_{int} = 0.0328), final R_1 = 0.0236, final wR_2 = 0.0487, GoF = 1.023.

UV−Vis Titrations. UV−vis spectroscopy was performed on a Varian Cary 50 photospectrometer using 1 cm quartz cuvettes. After a pure solvent background scan, a solution of 0.5 mM [Ir] in 4:1 H_2O/^{t}BuOH (2.5 mL) was added to the cuvette and a spectrum acquired (every 30 s for 1 h, 300−900 nm spectral range, 1 nm resolution, 2400 nm/min scan rate). The solution in the cuvette was removed and added to a small vial with preweighed KCl. Once the KCl had dissolved the solution was returned to the cuvette and a new spectrum taken. This procedure was repeated for 50, 100, 200, 400, and 800 equiv of KCl (75 μmol, 150 μmol, 0.3 mmol, 0.6 mmol, and 1.2 mmol, respectively).

UV−Vis Activation Studies. After a pure solvent background scan, a solution of 0.75 mM [Ir] in 4:1 H_2O/^{t}BuOH (2.5 mL) was added to a quartz cuvette containing a small magnetic stir bar. The solution was stirred, and automatic acquisition of spectra was started (every 30 s for 1 h, 300−900 nm spectral range, 1 nm resolution, 2400 nm/min scan rate). After the first scan, $NaIO_4$ (0.15 M, 0.5 mL in H_2O) was added and the reaction left to proceed while spectra acquisition continued. Single-wavelength kinetic runs were performed using the same protocol but following intensity at a selected wavelength with 0.1 Hz resolution.

EBS Oxidation. *pH Dependence.* A solution of ethylbenzenesulfonic acid and NaOH (0.1 mM in H_2O, 2 mL, pH adjusted to the desired value) was added to a [Ir] solution (5 mM in 4:1 H_2O/^{t}BuOH, 0.4 mL) in a screw-cap vial and stirred at 25 °C. A further 1 mL of H_2O and 1 mL of ^{t}BuOH were added to give a total volume of 4.4 mL. The reaction was initiated by the addition a solution of $NaIO_4$ (1 mL, 0.1 mM in H_2O). The reaction was quenched after 5 min by addition of $NaHSO_3$ (1 M, 2 mL). An aliquot of the solution was taken, D_2O added, and the sample analyzed by ^{1}H NMR spectroscopy to give conversion by relative peak area integration of the aromatic protons of starting material (400 MHz, D_2O: δ = 7.63, 7.61, 7.32, 7.30) vs product (400 MHz, D_2O: δ = 8.02, 8.00, 7.84, 7.82) as in the literature.[29]

Solvent Variation. Kinetic data were collected *in situ* using 5 mm NMR sample tubes. $NaIO_4$ (0.1 mmol) in 0.2 mL of D_2O, EBS (0.02 mmol) in 0.2 mL of H_2O, and the desired cosolvent (0.1 mL) were added to the NMR tube. After a background spectrum was taken, the [Ir1] precatalyst was added (2 μmol) and periodic ^{1}H spectra collection started. The time between the addition of [Ir] and the first scan was recorded and incorporated into the kinetic data. Cosolvents tested included ^{t}BuOH, acetone, MeCN, nitromethane, HMPA, and DMA. In the case where no cosolvent was added, a further 0.1 mL of D_2O was used.

Precatalyst Variation. Kinetic data were collected *in situ* using 5 mm NMR sample tubes. $NaIO_4$ (0.1 mmol) in 0.2 mL of D_2O, EBS (0.02 mmol) in 0.2 mL of H_2O, and ^{t}BuOH (0.1 mL) were added to the NMR tube. After a background spectrum was taken, the [Ir] precatalyst was added (2 μmol) and periodic ^{1}H spectra collection started. The time between the addition of [Ir] and the first scan was recorded and incorporated into the kinetic data.

Additional $NaIO_4$. Initial reaction was carried out at 0.04 mmol EBS, 0.2 mmol $NaIO_4$, 0.2 μmol, 1 mol% [Ir5] at pH 7, 25 °C in 4:1 H_2O/^{t}BuOH solvent mixture, and the NMR tube was left at room temperature for 200 min. ^{1}H NMR spectra were recorded to check the reaction had plateaued before a second addition of $NaIO_4$ was made (a further 0.2 mL of 1 M solution = another 0.2 mmol) and periodic ^{1}H spectra collection started.

Water Oxidation. *In situ* oxygen evolution data were collected using a Hansatech Oxygraph Plus system with a DW2/2 Clark-type electrode chamber (with temperature control and magnetic stirring) measuring dissolved O_2 in solution. The electrode was prepared with 0.1 M KCl electrolyte under a PTFE membrane and spacer paper, and the instrument was zeroed with 10 μM $NaIO_4$ solution in H_2O (2 mL) thoroughly degassed with argon. Oxygen evolution data were collected under the exact same conditions as used for the CH oxidation (200 mM $NaIO_4$, 40 mM EBS, 1 mol% [Ir] in ^{t}BuOH/H_2O/D_2O (1:2:2), with initiation by addition of [Ir] (120 μL of a 5 mM solution of [Ir] in H_2O/20% ^{t}BuOH).

All experiments were conducted at 25 °C, with data collected at 10 Hz, and run in triplicates with initial rates derived from the average.

■ ASSOCIATED CONTENT

Supporting Information

The Supporting Information is available free of charge on the ACS Publications website at DOI: 10.1021/acs.organomet.7b00492.

Further experimental and analytical data including NMR spectra, additional UV−vis plots, and crystallographic details (PDF)

Accession Codes

CCDC 1413039−1413044 contain the supplementary crystallographic data for this paper. These data can be obtained free of charge via www.ccdc.cam.ac.uk/data_request/cif, or by emailing data_request@ccdc.cam.ac.uk, or by contacting The Cambridge Crystallographic Data Centre, 12 Union Road, Cambridge CB2 1EZ, UK; fax: +44 1223 336033.

■ AUTHOR INFORMATION

Corresponding Author

*E-mail: u.hintermair@bath.ac.uk.

ORCID

Ulrich Hintermair: 0000-0001-6213-378X

Notes

The authors declare the following competing financial interest(s): U.S. Patent Application Number 14/317,906 by U.H. et al. contains intellectual property described in this article.

■ ACKNOWLEDGMENTS

This work was supported by a Research Grant from the Royal Society (Y0603) and the EPSRC Centre for Doctoral Training in Sustainable Chemical Technologies (EP/L016354/1). U.H. thanks the Centre for Sustainable Chemical Technologies for a Whorrod Research Fellowship. The authors would like to thank Prof. Frank Marken and Dr. Petra Cameron (University of

DOI: 10.1021/acs.organomet.7b00492
Organometallics XXXX, XXX, XXX−XXX

Bath) as well as Dr. Robert Potter (Johnson Matthey) for their support and assistance with this project.

REFERENCES

(1) White, M. C. *Science* **2012**, *335*, 807−809.
(2) Dick, A. R.; Sanford, M. S. *Tetrahedron* **2006**, *62*, 2439−2463.
(3) Gunay, A.; Theopold, K. H. *Chem. Rev.* **2010**, *110*, 1060−1081.
(4) Cook, G. K.; Mayer, J. M. *J. Am. Chem. Soc.* **1994**, *116*, 1855−1868.
(5) Cook, G. K.; Mayer, J. M. *J. Am. Chem. Soc.* **1995**, *117*, 7139−7156.
(6) Murahashi, S.-I.; Zhang, D. *Chem. Soc. Rev.* **2008**, *37*, 1490−1501.
(7) Zhou, M.; Crabtree, R. H. *Chem. Soc. Rev.* **2011**, *40*, 1875−1884.
(8) Suzuki, T. *Chem. Rev.* **2011**, *111*, 1825−1845.
(9) Borovik, A. S. *Chem. Soc. Rev.* **2011**, *40*, 1870−1874.
(10) Bordeaux, M.; Galarneau, A.; Drone, J. *Angew. Chem., Int. Ed.* **2012**, *51*, 10712−10723.
(11) Feng, J.-B.; Wu, X.-F. *Appl. Organomet. Chem.* **2015**, *29*, 63−86.
(12) Yeung, C. S.; Dong, V. M. *Chem. Rev.* **2011**, *111*, 1215−1292.
(13) Meyer, T. J.; Huynh, M. H. V. *Inorg. Chem.* **2003**, *42*, 8140−8160.
(14) Lindhorst, A. C.; Haslinger, S.; Kühn, F. E. *Chem. Commun.* **2015**, *51*, 17193−17212.
(15) Engelmann, X.; Monte-Pérez, I.; Ray, K. *Angew. Chem., Int. Ed.* **2016**, *55*, 7632−7649.
(16) Das, B.; Al-Hunaiti, A.; Haukka, M.; Demeshko, S.; Meyer, S.; Shteinman, A. a.; Meyer, F.; Repo, T.; Nordlander, E. *Eur. J. Inorg. Chem.* **2015**, *2015*, 3590−3601.
(17) Talsi, E. P.; Ottenbacher, R. V.; Bryliakov, K. P. *J. Organomet. Chem.* **2015**, *793*, 102−107.
(18) Kudrik, E. V.; Afanasiev, P.; Alvarez, L. X.; Dubourdeaux, P.; Clémancey, M.; Latour, J.-M.; Blondin, G.; Bouchu, D.; Albrieux, F.; Nefedov, S. E.; Sorokin, A. B. *Nat. Chem.* **2012**, *4*, 1024−1029.
(19) Wu, X.; Seo, M. S.; Davis, K. M.; Lee, Y.; Chen, J.; Cho, K.; Pushkar, Y. N.; Nam, W. *J. Am. Chem. Soc.* **2011**, *133*, 20088−20091.
(20) Ray, K.; Pfaff, F. F.; Wang, B.; Nam, W. *J. Am. Chem. Soc.* **2014**, *136*, 13942−13958.
(21) Garcia-Bosch, I.; Codolà, Z.; Prat, I.; Ribas, X.; Lloret-Fillol, J.; Costas, M. *Chem. - Eur. J.* **2012**, *18*, 13269−13273.
(22) Zhou, M.; Schley, N. D.; Crabtree, R. H. *J. Am. Chem. Soc.* **2010**, *132*, 12550−12551.
(23) Zhou, M.; Hintermair, U.; Hashiguchi, B. G.; Parent, A. R.; Hashmi, S. M.; Elimelech, M.; Periana, R. a.; Brudvig, G. W.; Crabtree, R. H. *Organometallics* **2013**, *32*, 957−965.
(24) Graeupner, J.; Hintermair, U.; Huang, D. L.; Thomsen, J. M.; Takase, M.; Campos, J.; Hashmi, S. M.; Elimelech, M.; Brudvig, G. W.; Crabtree, R. H. *Organometallics* **2013**, *32*, 5384−5390.
(25) Thomsen, J. M.; Huang, D. L.; Crabtree, R. H.; Brudvig, G. W. *Dalt. Trans* **2015**, *44*, 12452−12472.
(26) Hull, J. F.; Balcells, D.; Blakemore, J. D.; Incarvito, C. D.; Eisenstein, O.; Brudvig, G. W.; Crabtree, R. H. *J. Am. Chem. Soc.* **2009**, *131*, 8730−8731.
(27) Huang, D. L.; Beltrán-Suito, R.; Thomsen, J. M.; Hashmi, S. M.; Materna, K. L.; Sheehan, S. W.; Mercado, B. Q.; Brudvig, G. W.; Crabtree, R. H. *Inorg. Chem.* **2016**, *55*, 2427−2435.
(28) Sheehan, S. W.; Thomsen, J. M.; Hintermair, U.; Crabtree, R. H.; Brudvig, G. W.; Schmuttenmaer, C. A. *Nat. Commun.* **2015**, *6*, 6469.
(29) Zhou, M.; Balcells, D.; Parent, A. R.; Crabtree, R. H.; Eisenstein, O. *ACS Catal.* **2012**, *2*, 208−218.
(30) Betley, T. A.; Wu, Q.; Van Voorhis, T.; Nocera, D. G. *Inorg. Chem.* **2008**, *47*, 1849−1861.
(31) Blakemore, J. D.; Schley, N. D.; Balcells, D.; Hull, J. F.; Olack, G. W.; Incarvito, C. D.; Eisenstein, O.; Brudvig, G. W.; Crabtree, R. H. *J. Am. Chem. Soc.* **2010**, *132*, 16017−16029.
(32) Crabtree, R. H. *J. Chem. Soc. Dalt. Trans.* **2001**, 2437−2450.
(33) Dau, H.; Limberg, C.; Reier, T.; Risch, M.; Roggan, S.; Strasser, P. *ChemCatChem* **2010**, *2*, 724−761.
(34) Grotjahn, D. B.; Brown, D. B.; Martin, J. K.; Marelius, D. C.; Abadjian, M.; Tran, H. N.; Kalyuzhny, G.; Vecchio, K. S.; Specht, Z. G.; Cortes-llamas, S. A.; Miranda-soto, V.; van Niekerk, C.; Moore, C. E.; Rheingold, A. L. *J. Am. Chem. Soc.* **2011**, *133*, 19024−19027.
(35) Wang, C.; Wang, J.; Lin, W. *J. Am. Chem. Soc.* **2012**, *134*, 19895−19908.
(36) Hintermair, U.; Sheehan, S. W.; Parent, A. R.; Ess, D. H.; Richens, D. T.; Vaccaro, P. H.; Brudvig, G. W.; Crabtree, R. H. *J. Am. Chem. Soc.* **2013**, *135*, 10837−10851.
(37) Thomsen, J. M.; Sheehan, S. W.; Hashmi, S. M.; Campos, J.; Hintermair, U.; Crabtree, R. H.; Brudvig, G. W. *J. Am. Chem. Soc.* **2014**, *136*, 13826−13834.
(38) Ingram, A. J.; Wolk, A. B.; Flender, C.; Zhang, J.; Johnson, C. J.; Hintermair, U.; Crabtree, R. H.; Johnson, M. a; Zare, R. N. *Inorg. Chem.* **2014**, *53*, 423−433.
(39) Savini, A.; Belanzoni, P.; Bellachioma, G.; Zuccaccia, C.; Zuccaccia, D.; Macchioni, A. *Green Chem.* **2011**, *13*, 3360−3374.
(40) Zuccaccia, C.; Bellachioma, G.; Bolaño, S.; Rocchigiani, L.; Savini, A.; Macchioni, A. *Eur. J. Inorg. Chem.* **2012**, *9*, 1462−1468.
(41) Hintermair, U.; Hashmi, S. M.; Elimelech, M.; Crabtree, R. H. *J. Am. Chem. Soc.* **2012**, *134*, 9785−9795.
(42) Michaelos, T. K.; Shopov, D. Y.; Sinha, S. B.; Sharninghausen, L. S.; Fisher, K. J.; Lant, H. M. C.; Crabtree, R. H.; Brudvig, G. W. *Acc. Chem. Res.* **2017**, *50*, 952−959.
(43) Collins, J. *Acc. Chem. Res.* **1994**, *27*, 279−285.
(44) Crabtree, R. H. *J. Organomet. Chem.* **2014**, *751*, 174−180.
(45) Hintermair, U.; Campos, J.; Brewster, T. P.; Pratt, L. M.; Schley, N. D.; Crabtree, R. H. *ACS Catal.* **2014**, *4*, 99−108.
(46) Campos, J.; Hintermair, U.; Brewster, T. P.; Takase, M. K.; Crabtree, R. H. *ACS Catal.* **2014**, *4*, 973−985.
(47) White, C.; Yates, A.; Maitlis, P. M.; Heinekey, D. M. *Inorganic Synthesis* **1992**, *29*, 228−234.
(48) Schley, N. D.; Halbert, S.; Raynaud, C.; Eisenstein, O.; Crabtree, R. H. *Inorg. Chem.* **2012**, *51*, 12313−12323.
(49) Glueck, D. S.; Wu, J.; Hollander, F. J.; Bergman, R. G. *J. Am. Chem. Soc.* **1991**, *113*, 2041−2054.
(50) Noyori, R.; Yamakawa, M.; Hashiguchi, S. *J. Org. Chem.* **2001**, *66*, 7931−7944.
(51) Mayer, J. M. *Inorg. Chem.* **1988**, *27*, 3899−3903.
(52) Poth, T.; Paulus, H.; Elias, H.; Van Eldik, R.; Dücker-Benfer, C. *Eur. J. Inorg. Chem.* **2001**, *2001*, 1361−1369.
(53) Gersten, S. W.; Samuels, G. J.; Meyer, T. J. *J. Am. Chem. Soc.* **1982**, *104*, 4029−4030.
(54) Schley, N. D.; Blakemore, J. D.; Subbaiyan, N. K.; Incarvito, C. D.; D'Souza, F.; Crabtree, R. H.; Brudvig, G. W. *J. Am. Chem. Soc.* **2011**, *133*, 10473−10481.
(55) Plietker, B. *Synthesis* **2005**, *15*, 2453−2472.
(56) Mallat, T.; Baiker, A. *Catal. Sci. Technol.* **2011**, *1*, 1572−1583.

DOI: 10.1021/acs.organomet.7b00492
Organometallics XXXX, XXX, XXX−XXX